A hybrid enrichment strategy for the efficient construction of reduced order models by the proper generalized decomposition

Fabian Müller, Paul Baumanns and Kay Hameyer
Institute of Electrical Machines, RWTH Aachen University, Aachen, Germany

Received 30 August 2022
Revised 6 November 2022
16 February 2023
16 April 2023
Accepted 18 May 2023

Abstract

Purpose – The calculation of electromagnetic fields can involve many degrees of freedom (DOFs) to achieve accurate results. The DOFs are directly related to the computational effort of the simulation. The effort is decreased by using the proper generalized decomposition (PGD) and proper orthogonalized decomposition (POD). The purpose of this study is to combine the advantages of both methods. Therefore, a hybrid enrichment strategy is proposed and applied to different electromagnetic formulations.

Design/methodology/approach – The POD is an *a-priori* method, which exploits the solution space by decomposing reference solutions of the field problem. The disadvantage of this method is given by the unknown number of solutions necessary to reconstruct an accurate field representation. The PGD is an *a-priori* approach, which does not rely on reference solutions, but require much more computational effort than the POD. A hybrid enrichment strategy is proposed, based on building a small POD model and using it as a starting point of the PGD enrichment process.

Findings – The hybrid enrichment process is able to accurately approximate the reference system with a smaller computational effort compared to POD and PGD models. The hybrid enrichment process can be combined with the magneto-dynamic T-Ω formulation and the magnetic vector potential formulation to solve eddy current or non-linear problems.

Originality/value – The PGD enrichment process is improved by exploiting a POD. A linear eddy current problem and a non-linear electrical machine simulation are analyzed in terms of accuracy and computational effort. Further the PGD-AV formulation is derived and compared to the PGD-T-Ω reduced order model.

Keywords Model order reduction, Proper generalized decomposition, Proper orthogonal decomposition, Finite element method, Electrical machine

Paper type Research paper

1. Introduction

Electromagnetic simulations require a large computational effort, if transient effects, non-linear materials or many different parameter variations are considered in the study. To reduce the number of degrees of freedom (DOFs), model order reduction techniques, such as the proper orthogonalized decomposition (POD) or proper generalized decomposition (PGD), can be used (Chinesta *et al.*, 2013; Henneron and Clénet, 2016, 2017; Krimm *et al.*, 2019). While the first one is an *a-priori* approach with an optimal orthogonal basis, the latter one is an *a-priori* approach without the orthogonality property, even though they are closely related (Nouy, 2010). The particular aim of this scientific contribution is to analyze and

This work was supported by the German Research Foundation (DFG) within the research project number 347941356 "Numerical Analysis of Electromagnetic Fields by Proper Generalized Decomposition in Electrical Machines".

COMPEL - The international journal for computation and mathematics in electrical and electronic engineering

0332-1649
DOI 10.1108/COMPEL-08-2022-0289

clarify whether a combination of both techniques is possible and advantageous. To exploit the advantages of both methods, a numerical formulation combining POD and PGD is here presented. As an example of application two test cases are considered. A linear three-dimensional (3D) eddy current problem is first considered. Then, a two-dimensional (2D) problem consisting in a small synchronous machine including non-linear material is examined.

2. Fundamentals

2.1 Finite element formulations

For the numerical analysis with the finite element method (FEM), the electric and magnetic fields given by the Maxwell's equations are reformulated by introducing potentials. For eddy current problems, the AV formulation or the $T-\Omega$ formulation are mainly used (Hameyer and Belmans, 1999). The AV formulation represents the magnetic field by a vectorial and the electrical field by both scalar and vector potential. The $T-\Omega$ formulation uses a combination of scalar and vectorial potentials for the magnetic component and a vectorial one for the electric component. These and other conceivable potential are studied in detail in Kuczmann and Iványi (2008).

2.1.1 AV formulation. The magnetic vector potential formulation is based on equation (1), which express the magnetic flux density B as the curl of vector potential A and additionally a scalar potential V is introduced in equation (2) to ensure divergence-free eddy current regions:

$$\nabla \times \boldsymbol{A} = \boldsymbol{B}, \tag{1}$$

$$\nabla \cdot \left(\sigma \left(\frac{\partial \boldsymbol{A}}{\partial t} - \nabla V \right) \right) = 0 \ . \tag{2}$$

In a 2D analysis, the electrical scalar potential is not considered. Using the material constitutive laws into Ampère's and Faraday's law, the strong form of the system can be determined. Consecutively, the weak form of this differential equation is derived by using Galerkin's method to achieve a solvable form in the discretized domain D (Hameyer and Belmans, 1999; Kuczmann and Iványi, 2008). Assuming Dirichlet conditions on the boundary of the domain with a fixed potential of zero results in:

$$\int_{\mathrm{D}} \nu(\nabla \times w) \cdot (\nabla \times A) + w \cdot \left(\frac{\sigma \partial \boldsymbol{A}}{\partial t} + \sigma \cdot \nabla V \right) \, d\mathrm{D} = \int_{D} w \cdot \boldsymbol{J}_s d\mathrm{D}, \tag{3}$$

$$\int_{\mathrm{D}} \sigma \nabla w \cdot \left(\frac{\partial \boldsymbol{A}}{\partial t} + \nabla V \right) d\mathrm{D} = 0 \ , \tag{4}$$

Where σ is the electric conductivity and $v = 1/\mu$ is the magnetic reluctivity. Hereby, w denotes the element test function and J_{S} is the source current density. The test functions for equation (3) are edge elements, whereas those in equation (4) are nodal elements.

2.1.2 $T-\Omega$ formulation. In contrast to the AV formulation, in the $T-\Omega$ formulation a vector electric potential and a scalar potential for the representation of the magnetic field are used. The magnetic field is expressed by:

$$\boldsymbol{H} = \boldsymbol{T} - \nabla\,\Omega, \tag{5}$$

where the electric vector potential $\boldsymbol{T}$ is given by the sum of the exciting vector potential $\boldsymbol{T}_S$ and the eddy current component $\boldsymbol{T}_e$, which is only defined in the conductive regions:

$$\boldsymbol{T} = \boldsymbol{T}_S + \boldsymbol{T}_e\ , \tag{6}$$

$$\nabla \times \boldsymbol{T}_S = \boldsymbol{J}_S, \tag{7}$$

$$\nabla \times \boldsymbol{T}_e = \boldsymbol{J}_e. \tag{8}$$

The source electric vector potential has to be determined before solving the field problem. To achieve $\boldsymbol{T}_S$, a tree-cotree technique is used (Boehmer *et al.*, 2013), which makes it possible to represent the source current density $\boldsymbol{J}_S$. These potentials are substituted into Faraday's and Gauß' laws and combined with material laws. Again, the weak form is derived by Galerkin's method as:

$$\int_D \frac{1}{\sigma}(\nabla \times w)\cdot(\nabla \times \boldsymbol{T}_e) + \frac{w\cdot\partial\mu\boldsymbol{T}_e - w\cdot\partial\mu\nabla\,\Omega}{\partial t}\ d\mathrm{D} = -\int_D \frac{w\cdot\partial\mu\boldsymbol{T}_S}{\partial t}\ d\mathrm{D} \tag{9}$$

$$\int_D -\mu\nabla w\cdot\boldsymbol{T}_e + \mu\nabla w\cdot\nabla\,\Omega\ d\mathrm{D} = \int_D \mu\nabla w\cdot\boldsymbol{T}_S\ d\mathrm{D} \tag{10}$$

Similar to the test functions in equation (3), the test functions in equation (9) are taken from the edge element space for 3D analysis. The test functions of equation (10) are taken from the nodal element space such as those for discretizing equation (4).

In general and independently from the $T-\Omega$ formulation, the system of interest can be rewritten as a differential algebraic equation (DAE) in the form of:

$$\boldsymbol{M}\boldsymbol{X}(t) + \boldsymbol{K}\frac{\mathrm{d}\boldsymbol{X}(t)}{\mathrm{d}t} = \boldsymbol{F}(t)\ , \tag{11}$$

Where $\mathbf{M}$ denotes the mass matrix, $\mathbf{K}$ is the stiffness matrix and $\boldsymbol{F}(t)$ is the load vector. The unknown vector $\boldsymbol{X}(t)$ belongs to $\mathbb{R}^n$, where n is the number of DOFs.

2.2 Model order reduction techniques

The following model order reduction techniques are based on the separation of variables into sums over function products, which only depend on a single parameter each (Nouy, 2010). For an arbitrary potential $\boldsymbol{U}(x,t)$, the separation is given by:

$$\boldsymbol{U}(x,t) \approx \sum_{i=1}^{m} \boldsymbol{R}_{i,U}(x)S_{i,U}(t) \tag{12}$$

The variables here are the space x and the time t. The subscript $\boldsymbol{U}$ denotes to which potential the function $\boldsymbol{R}$ and S belong. Other parameters such as the excitation in electrical machines,

given by permanent magnet remanence or current angle and amplitude in the dq-frame can be introduced into the decomposition as well, which enables the fast study of the machine behavior by model order reduction techniques (Müller *et al.*, 2020a, 2020b, 2021, 2022).

2.2.1 Proper orthogonal decomposition. The POD as an *a-posteriori* method relies on the knowledge of the solution subspace of the reference system. The fundamental principle of the POD is based on the projection of the reference problem into a subspace, which is deduced from solutions of the reference system. These solutions are computed beforehand and are called snapshots, here denoted by X. The snapshots are decomposed into a set of orthogonal vectors, which are consecutively used to create a projection operator (Chinesta *et al.*, 2011; Clénet *et al.*, 2015; Montier *et al.*, 2017). To obtain this operator, first some snapshots are collected into:

$$\boldsymbol{A}_{\mathrm{S}} = [X_1, \ldots, X_{\mathrm{NoS}}] \tag{13}$$

Then the operator $\boldsymbol{\Psi}$, which maps the reference system into a subspace, spanned by the orthogonal basis vectors, is achieved for, e.g. by taking the left singular vectors of the snapshot matrix.

Due to the fact that the projection operator is built by the snapshot method, it is crucial to enrich the most important information of the solution subspace of the system into the snapshots to ensure a good approximation (Müller *et al.*, 2020a, 2020b, 2021, 2022). This underlines the advantage and disadvantage of this method: the effort of a single snapshot computation is acceptable, but it is not known *a-priori* which and how many snapshots are required for an accurate reduced model. In Mukherjee *et al.* (2017), a greedy algorithm is combined with the POD to alleviate this problem. Particularly for transient problems, this can lead to a large additional computational effort. Another way to enrich information into the reduced basis without the need of a singular value decomposition is given by (Kasolis and Clemens, 2020). It is based on statistics and evaluates the information entropy of the snapshots. Particularly, for large models this approach reduces the effort associated with the computation of singular vectors. The POD constructs a Reduced Order Model (ROM) of order $m \backslash \!\!\!\ll n$ by the projection of equation (11) into a reduced subspace spanned by the snapshots:

$$\boldsymbol{\Psi}^{\mathrm{t}}\mathbf{M}\boldsymbol{\Psi}\boldsymbol{X}_{\mathrm{r}}(t) + \boldsymbol{\Psi}^{\mathrm{t}}\mathbf{K}\boldsymbol{\Psi}\frac{\mathrm{d}\boldsymbol{X}_{\mathrm{r}}(t)}{\mathrm{d}t} = \boldsymbol{\Psi}^{t}\boldsymbol{F}(t)\ . \tag{14}$$

The full solution vector is then given by the multiplication of projection operator with the reduced solution $\boldsymbol{X} = \boldsymbol{\Psi}\boldsymbol{X}_{\mathrm{r}}$. This method is independent of the type of potentials used for the discretization and it is non-intrusive because the PDE is left unchanged. Different methods exist to construct the projection, on one hand one projection operator for the whole solution vector can be created or a separate operator for each potential (Montier *et al.*, 2017). In this contribution only one projection operator for the whole system is used.

If non-linearities have to be considered a similar approach, i.e. the Discrete Empirical Interpolation Method (DEIM), can be used together with the POD and PGD (Chaturantabut and Sorensen, 2010; Henneron and Clénet, 2016, 2017, Müller *et al.*, 2020a, 2020b, 2021, 2022). It collects the non-linearity in a second snapshot matrix, which is analogously decomposed as in the POD. By applying a greedy algorithm (Chaturantabut and Sorensen, 2010), a subset of elements can be determined on which the non-linearity has to be evaluated. Afterward the projection operator of the DEIM is used to interpolate the non-linearity of these subset of elements into the domains with non-linear media.

2.2.2 Proper generalized decomposition. The PGD is an *a-priori* approach and is based on a direct decomposition of the unknown potential $\boldsymbol{U}$ into a sum of functional products. In contrast to the POD, the PGD only requires to build an operator given by the weak forms of the partial differential equations and hence it does not require the knowledge of the solution space by decomposing previously computed solutions. The terms of the sum are in the following also referred to as modes (Nouy, 2010; Chinesta *et al.*, 2011; Chinesta *et al.*, 2013). In the following, the transient problem is used to explain the enrichment strategy of the PGD. Test functions are separated as potentials in equation (12), that is:

$$w_{\boldsymbol{U}} = \boldsymbol{R}^{*}{}_{m,\boldsymbol{U}}(\boldsymbol{x})S_{m,\boldsymbol{U}}(t) + \boldsymbol{R}_{m,\boldsymbol{U}}(\boldsymbol{x})S^{*}_{m,\boldsymbol{U}}(t) \ . \tag{15}$$

To identify a couple of these functions for a particular mode m, an Alternative Direction Scheme (ADS) is used (Nouy, 2010), also called power iteration. By assuming the modes up to $m-1$ are known, the ADS starts with the initialization of the function $S_{m,\boldsymbol{U}} = S_{m-1,\boldsymbol{U}}$. If m is equal to one, S_m is initialized with the temporal evolution of the exciting current. Consecutively, one of the unknown functions is taken as fixed and the other function is computed. The modes $\boldsymbol{R}$ related to the space are collected in $B_{\boldsymbol{R}}$, which represent the space basis and the time modes S are collected in the time basis B_S. The whole enrichment process is denoted in Algorithm 1.

Algorithm 1: PGD enrichment process.

1: $m = 1$, $B_{\boldsymbol{R}} = []$, $B_S = []$
2: While $m \leq m_{\max}$ and $error > \epsilon$
3: Initialise $S(t)$, $k = 1$
4: While $k < k_{\max}$ and $rel.change > \epsilon_{rel}$
5: Compute $\boldsymbol{R}_m = g(S)$
6: Compute $S_m = h(\boldsymbol{R})$
7: Compute relative change of $\boldsymbol{R}_m$ and S_m
8: End while
9: Add $\boldsymbol{R}_m \rightarrow B_{\boldsymbol{R}}$ and $S_m \rightarrow B_S$
10: $\boldsymbol{U}_m(\boldsymbol{x},t) = \boldsymbol{U}_{m-1}(\boldsymbol{x},t) + \boldsymbol{R}_m(\boldsymbol{x})S_m(t)$
11: Compute error
12: End while

Hereby, the error used in Step 2 can be chosen as whether the absolute residual or other criteria, such as the error of the eddy current losses (Müller *et al.*, 2020a, 2020b, 2021, 2022). If two potentials exist, such as in the AV formulation or $T-\Omega$ formulation, the operators $g(S)$ and $h(\boldsymbol{R})$ compute two space modes $\boldsymbol{R}_m$ and time modes S_m. $B_{\boldsymbol{R}}$ and B_S contain the computed space and time modes, $m_{\max}$ denotes the maximum number of modes and $k_{\max}$ the maximum number of iterations of the ADS. The power iteration is given by lines four to nine in Algorithm 1. This process enables to enrich eigenfunctions of the problem with high information content (Nouy, 2010). To avoid ambiguity, it is important to normalize all functions except for one. In this example the time function S is normalized, but normalization of the spatial part works equivalently. The function's operators $g(S)$ and $h(\boldsymbol{R})$, built by the PGD, arise from the system of equations given by the differential equations to be solved. Therefore, the PGD is an intrusive approach, contrary to the POD. After the enrichment process, commonly denoted as offline-phase, is converged, the field quantities and the post processing can be quickly evaluated. This second phase is named "online-phase".

2.2.2.1 Proper generalized decomposition-AV formulation. To achieve the operators for the AV formulation, the separation approach [equation (12)] is introduced to both potentials and the related test functions in the nodal and edge element space [equation (15)].

$$\sum_{i=1}^{m}\int_{\mathrm{T}} S_{m,A}S_{i,A}dt\int_{\mathrm{D}}\nu\left(\nabla\times R^{*}_{m,A}\right)\cdot\left(\nabla\times R_{i,A}\right)d\mathrm{D}+\sum_{i=1}^{m}\int_{\mathrm{T}} S_{m,A}\frac{dS_{i,A}}{dt}dt\int_{\mathrm{D}}\sigma R^{*}_{m,A}\cdot R_{i,A}d\mathrm{D}$$
$$+\sum_{i=1}^{m}\int_{\mathrm{T}} S_{m,A}S_{i,V}dt\int_{\mathrm{D}}\sigma R^{*}_{m,A}\cdot\nabla R_{i,V}d\mathrm{D}-\int_{\mathrm{T}} S_{m,A}J_{\mathrm{S,T}}dt\int_{\mathrm{D}} R^{*}_{m,A}J_{\mathrm{S},\boldsymbol{x}}d\mathrm{D}=0 \tag{16}$$

$$\sum_{i=1}^{m}\int_{\mathrm{T}} S_{m,V}\frac{dS_{i,A}}{dt}dt\int_{\mathrm{D}}\sigma\nabla R^{*}_{m,V}\cdot R_{i,A}d\mathrm{D}+\int_{\mathrm{T}} S_{m,V}S_{i,V}dt\int_{\mathrm{D}}\sigma\nabla R^{*}_{m,V}\cdot\nabla R_{i,V}d\mathrm{D}=0 \tag{17}$$

Sorting the integrals regarding the time and space domain results in the following operator $g(S)$ given by equations (16) and (17). $g(S)$ states a system of equations resulting from the coupled differential equations (3) and (4) to compute the space function $\boldsymbol{R}_m$ and is solved by the FEM.

$$\sum_{i=1}^{m}\int_{\mathrm{T}} S^{*}_{m,A}S_{i,A}dt\int_{\mathrm{D}}\nu\left(\nabla\times R_{m,A}\right)\cdot\left(\nabla\times R_{i,A}\right)d\mathrm{D}+\sum_{i=1}^{m}\int_{\mathrm{T}} S^{*}_{m,A}\frac{dS_{i,A}}{dt}dt\int_{\mathrm{D}}\sigma R_{m,A}\cdot R_{i,A}d\mathrm{D}$$
$$+\sum_{i=1}^{m}\int_{\mathrm{T}} S^{*}_{m,A}S_{i,V}dt\int_{\mathrm{D}}\sigma R_{m,A}\cdot\nabla R_{i,V}d\mathrm{D}-\int_{\mathrm{T}} S^{*}_{m,A}J_{\mathrm{S,T}}dt\int_{\mathrm{D}} R_{m,A}\cdot J_{\mathrm{S},\boldsymbol{x}}d\mathrm{D}=0 \tag{18}$$

$$\sum_{i=1}^{m}\int_{\mathrm{T}} S^{*}_{m,V}\frac{dS_{i,A}}{dt}dt\int_{\mathrm{D}}\sigma\nabla R_{m,V}\cdot R_{i,A}d\mathrm{D}+\int_{\mathrm{T}} S^{*}_{m,V}S_{i,V}dt\int_{\mathrm{D}}\sigma\nabla R_{m,V}\cdot\nabla R_{i,V}d\mathrm{D}=0 \tag{19}$$

After the spatial mode $\boldsymbol{R}_m$ is calculated, the operator $h(\boldsymbol{R})$ for the computation of the time modes is given by equations (18) and (19). The operator consists of two coupled ordinary differential equations (ODE). The integrals over the domain D are computed on the mesh and result in scalar coefficients for the ODE. Equations (18) and (19) can for example be solved by a one-dimensional FEM or by reformulation into a strong form (Müller *et al.*, 2020a, 2020b, 2021, 2022).

2.2.2.2 Proper generalized decomposition-T $-$ $\boldsymbol{\Omega}$ formulation. Analogously to the PGD-AV formulation, the operators of the PGD in combination with the magneto dynamic scalar potential formulation are deduced. The spatial operator $g(S)$ is defined as the system of equations given by equations (20) and (21):

$$\sum_{i=1}^{m}\int_{\mathrm{T}} S_{m,T_e}S_{i,T_e}dt\int_{\mathrm{D}}\frac{1}{\sigma}\left(\nabla\times R_{i,T_e}\right)\cdot\left(\nabla\times R^{*}_{m,T_e}\right)d\mathrm{D}+\int_{\mathrm{T}} S_{m,T_e}\frac{dS_{i,T_e}}{dt}dt\int_{\mathrm{D}}\mu R_{i,T_e}\cdot R^{*}_{m,T_e}d\mathrm{D}$$
$$-\sum_{i=1}^{m}\int_{\mathrm{T}} S_{m,T_e}\frac{dS_{i,\,\Omega}}{dt}dt\int_{\mathrm{D}}\mu\nabla R_{i,\,\Omega}\cdot R^{*}_{m,T_e}dD+\int_{\mathrm{T}} S_{m,T_e}\frac{dT_{\mathrm{S,T}}}{dt}dt\int_{\mathrm{D}}\mu T_{\mathrm{S},\boldsymbol{x}}\cdot R^{*}_{m,T_e}d\mathrm{D}=0 \tag{20}$$

$$\sum_{i=1}^{m}\int_{\mathrm{T}} S_{m,\,\Omega}S_{i,T_e}dt\int_{\mathrm{D}} -\mu R_{i,T_e}\cdot\nabla R^{*}_{m,\,\Omega}d\mathrm{D}+\int_{\mathrm{T}} S_{m,\,\Omega}S_{i,\,\Omega}dt\int_{\mathrm{D}}\mu\nabla R_{i,\,\Omega}\cdot\nabla R^{*}_{m,\,\Omega}d\mathrm{D}$$
$$-\int_{\mathrm{T}} S_{m,\,\Omega}T_{\mathrm{S,T}}dt\int_{\mathrm{D}}\mu T_{\mathrm{S},\boldsymbol{x}}\cdot\nabla R^{*}_{m,\,\Omega}d\mathrm{D}=0 \tag{21}$$

And the operator $h(\boldsymbol{R})$ for the time functions is defined as the system of equations given by equations (22) and (23):

$$\sum_{i=1}^{m}\int_{\mathrm{T}} S^{*}_{m,T_e}S_{i,T_e}dt\int_{\mathrm{D}}\frac{1}{\sigma}\left(\nabla\times R_{i,T_e}\right)\cdot\left(\nabla\times R_{m,T_e}\right)d\mathrm{D}+\int_{\mathrm{T}} S^{*}_{m,T_e}\frac{dS_{i,T_e}}{dt}dt\int_{\mathrm{D}}\mu R_{i,T_e}\cdot R_{m,T_e}d\mathrm{D}$$
$$-\sum_{i=1}^{m}\int_{\mathrm{T}} S^{*}_{m,T_e}\frac{dS_{i,\,\Omega}}{dt}dt\int_{D}\mu\nabla R_{i,\,\Omega}\cdot R_{m,T_e}dD+\int_{\mathrm{T}} S^{*}_{m,T_e}\frac{dT_{\mathrm{S,T}}}{dt}dt\int_{D}\mu T_{\mathrm{S},\boldsymbol{x}}\cdot R_{m,T_e}d\mathrm{D}=0\ , \tag{22}$$

$$\sum_{i=1}^{m}\int_{\mathrm{T}} S^{*}_{m,\,\Omega}S_{i,T_e}dt\int_{\mathrm{D}} -\mu R_{i,T_e}\cdot\nabla R_{m,\,\Omega}dD+\int_{\mathrm{T}} S^{*}_{m,\,\Omega}S_{i,\,\Omega}dt\int_{\mathrm{D}}\mu\nabla R_{i,\,\Omega}\cdot\nabla R_{m,\,\Omega}d\mathrm{D}$$
$$-\int_{\mathrm{T}} S^{*}_{m,\,\Omega}T_{\mathrm{S,T}}dt\int_{\mathrm{D}}\mu T_{\mathrm{S},\boldsymbol{x}}\cdot\nabla R_{m,\,\Omega}d\mathrm{D}=0\ . \tag{23}$$

3. Hybrid enrichment strategy

In Nouy (2010), it is noted that the PGD is an *a-priori* and generalized version of the POD. Further, it is explained that the columns of the POD projection operator $\boldsymbol{\Psi}$ are the space modes of the decomposition. The hybrid enrichment strategy consists of a two-stage process: The reference system is solved for a distinct number of steps and subsequently the solutions are decomposed to achieve the operator $\boldsymbol{\Psi}\in\mathbb{R}^{\mathrm{DOF}\times NoS}$. Then f columns are handed over to the PGD to serve as a startup solution of the first f space modes and assumed to be fixed. Therefore, only the operator $h(\boldsymbol{R})$ has to be computed. After m becomes large than f, the standard PGD enrichment process continues by computing both operators $g(S)$ and $h(\boldsymbol{R})$. The complete process is given in Algorithm 2.

Algorithm 2: Hybrid enrichment process.

```
Construct Ψ from snapshots and initialize m=1,
B_R = Ψ[:,1:f], B_S = []
While m ≤ m_max and error > ϵ
    Initialise S(t), k = 1
    While k < k_max and rel.change > ϵ_rel
        If m ≤ f : R_m = column m of Ψ
        Else: Compute R_m = g(S)
        End If
        Compute S_m = h(R)
        Compute relative change of R_m and S_m
```

```
End while
Add R_m → B_R and S_m → B_S
U_m(x,t) = U_{m−1}(x,t) + R_m(x)S_m(t)
Compute error
End while
```

Although the hybrid enrichment process is not an *a-priori* approach, interfering with the generalization approach of the PGD of lifting the requirement for previously computed solutions, it has certain advantages. First, the columns of $\boldsymbol{\Psi}$ span an orthogonal system and, second, the number of finite element computations related to solving large systems of equations can be decreased.

4. Application

4.1 Three dimensional linear eddy current problems

The first application example consists of a conducting sample placed in a short coil, shown in Figure 1. The conductivity is set to 40 MS/m and the frequency is 50 Hz. The excitation is given by a sinusoidal signal with a current amplitude of 1,000 A. The studied time interval spans two full periods and is sampled with 150 steps per period. The problem is computed with the POD, PGD and hybrid approach for both formulations to analyze the reduction, accuracy and feasibility of the approaches. The reference solutions used in the following sections are obtained by 3D transient finite element simulations with the AV formulation and $T - \Omega$ formulation. The utilized elements are of first order. The relative error of the Joule losses is calculated between the reference 3D simulation and those using model reduction techniques.

4.1.1 $T - \Omega$ formulation. In Figure 2, the results for the simulation with the $T - \Omega$ formulation are given in terms of Joule losses versus time. As snapshots for the POD, the solutions for the first few consecutive time steps are taken. For the first comparison the hybrid approach here uses the first two snapshots of the POD basis. A comparison of the influence of the number of snapshots used in the hybrid approach is subsequently presented. As described in Müller *et al.* (2020a, 2020b, 2021, 2022), the POD reduced order model [Figure 2(a)] does not approximate the reference losses well, due to the slowly increasing information content of the snapshots in transient problems. The PGD in Figure 2(b) shows a better approximation of the reference losses by using 6 modes. The hybrid approach in Figure 2(c) starts with two space modes extracted from $\boldsymbol{\Psi}$, built by the first six consecutive snapshots. It shows that the hybrid enrichment process produces less accurate losses over time compared to the pure PGD, but the

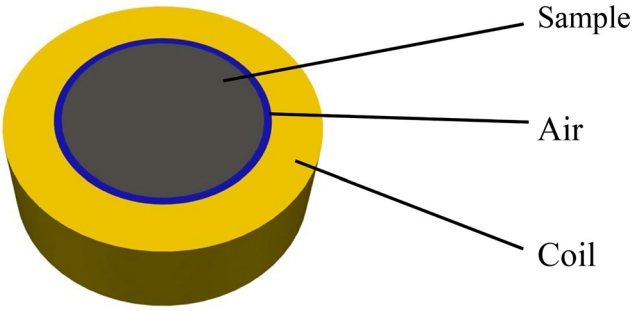

Source: Authors' own work

Figure 1.
Geometry of the transient eddy current problem

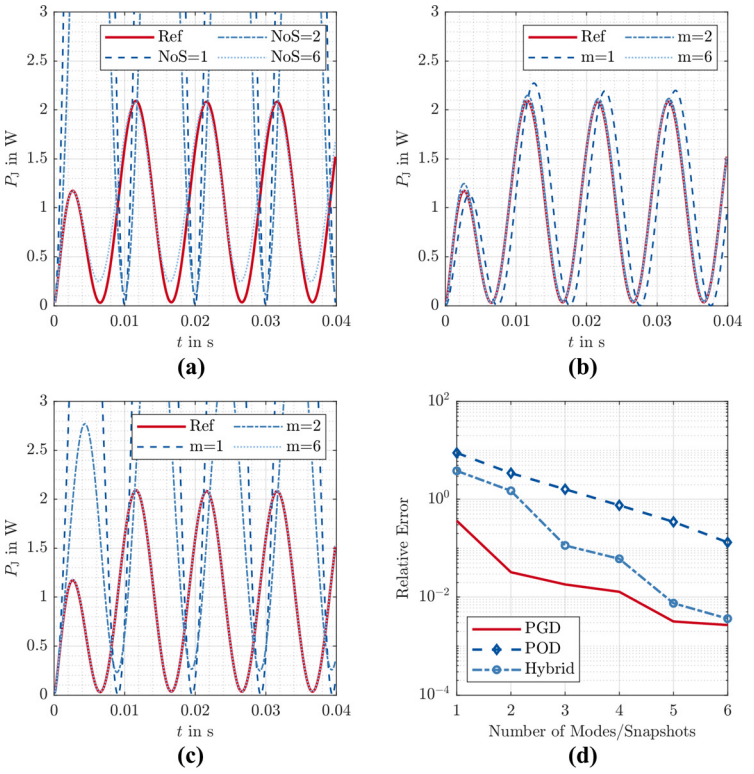

Notes: (a) POD; (b) PGD; (c) Hybrid; (d) relative error versus number of modes/snapshots

Source: Authors' own work

Figure 2.
Joule losses for the transient problem simulated with the $T - \Omega$ formulation

results are closer to the reference than for the POD approach. In Figure 2(d), the relative error is depicted: The hybrid approach convergence is located in between the POD and PGD method and the PGD more accurate than the POD.

In Figure 3, the relative error of the number of columns of $\boldsymbol{\Psi}$, used in the hybrid approach, on the convergence is pictured. For both studies, the same snapshots are taken for the construction of $\boldsymbol{\Psi}$ and the number of columns is varied. The results highlight the decreasing information value of the singular vectors contained in $\boldsymbol{\Psi}$, which reflects in the hybrid approaches convergence behavior. Taking more columns into account worsens the convergence and thus the accuracy of the fifth mode is worse than the POD approximation. The results highlight the decreasing information value of the singular vectors contained in $\boldsymbol{\Psi}$, which reflects in the hybrid approaches convergence behavior. Taking more columns into account worsens the convergence and thus the accuracy of the fifth mode is worse than the POD approximation. The enrichment process computes modes, which minimize the error over the whole time interval, while the POD basis vectors minimize the error in the subspace spanned by the snapshots. Taking sequential snapshots only represents a small part of the time interval. The operator $h(\boldsymbol{R})$ given by equations (22), (23) tries then to minimize the error over the whole time interval with space modes taken

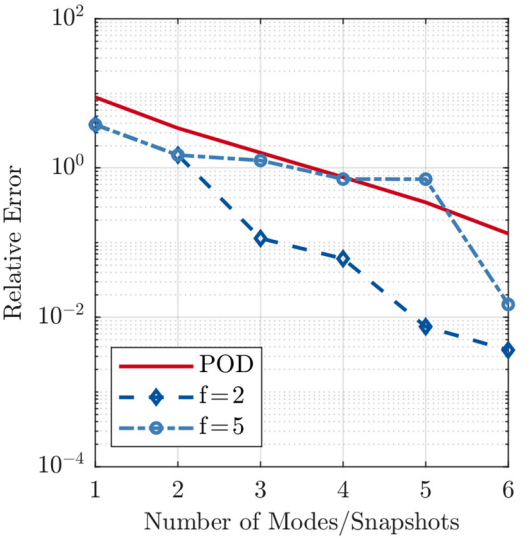

Figure 3.
Relative error of the Joule losses of the hybrid approach for different number of snapshots

Source: Authors' own work

from the subspace spanned by the POD basis, which results for a worsened convergence if more POD snapshots are used. After the fifth mode m is bigger than the number of used POD basis vectors and therefore, the next space mode is computed from the operator $g(S)$ given by equations (20), (21). This space mode improves, especially the approximation of the time interval, which is not included in the POD snapshots. This indicates that required number of modes in the hybrid approach to accurately approximate the system is influenced by the decreasing information content of the snapshots.

4.1.2 AV formulation. For the case study, using the AV formulation, a similar behavior of the Joule losses versus time can be observed for the POD [Figure 4(a)] and PGD [Figure 4(b)] compared to the $T-\Omega$ formulation. The POD converges slower toward the reference losses than the PGD, but the PGD in combination with the magnetic vector and electric scalar potential requires more modes than the PGD using an electric vector potential and a scalar magnetic potential. Comparing Figure 2(d) and Figure 4(d) reveals that the ROM with the $T-\Omega$ potentials converge smoother toward the reference solutions than the ROMs using the AV potentials, particularly for the POD. Again, the PGD shows a more accurate approximation of the system compared to the POD. Further, it has to be mentioned that the hybrid approach in combination with AV potentials diverges. To receive a converging model, Algorithm 2 has to be adapted to initialize $\boldsymbol{R}_m$ with the corresponding column of $\boldsymbol{\Psi}$ and consecutively solve both operators $g(S)$ and $h(\boldsymbol{R})$ instead of only $h(\boldsymbol{R})$ for all modes and not only $m > f$, which contradicts the original idea of the hybrid approach. This adaption results in a process, which is very similar to the standard PGD enrichment given in Algorithm 1 with an initialization of the space mode $\boldsymbol{R}_m$ instead of S_m. Further, it is necessary to exchange the computation of $g(S)$ and $h(\boldsymbol{R})$. This results in the very similar results of the losses for the PGD and the hybrid model. The results of this section show that the POD and PGD can be combined with the AV formulation, but the hybrid enrichment procedure is unstable with the AV formulation. Applying the described adaption led to a converging model, which conflicts with the basic idea of the hybrid approach of not calculating $g(S)$ for $m \leq f$.

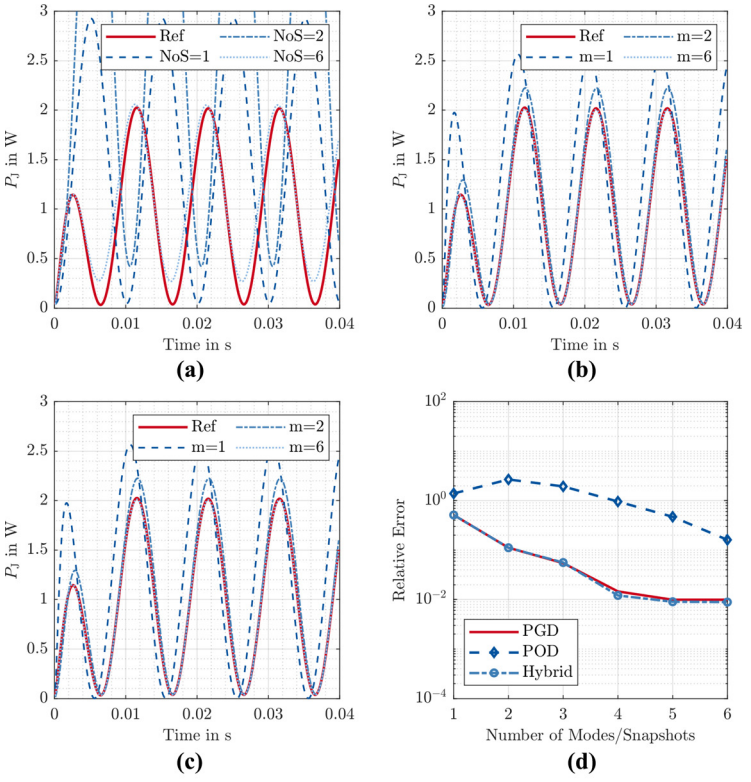

Notes: (a) POD; (b) PGD; (c) Hybrid; (d) relative error versus number of modes/snapshots

Source: Authors' own work

Figure 4.
Joule losses for the transient problem simulated with the *A V* formulation

4.2 Non-linear simulation of an electrical machine with a locked rotor

A non-linear electrical machine is now analyzed with the PGD, POD and hybrid approach in combination with the magnetic vector potential formulation in two dimensions (Müller *et al.*, 2020a, 2020b, 2021, 2022). This analysis is conducted on a surface permanent magnet synchronous machine shown in Figure 5. The magnet remanence is set to 1.2 T and the excitation current holds an amplitude of 5 A. The rotor is locked in position and the electric angle is divided into 73 steps for one electrical period. The flux guiding material in the stator and rotor holds a non-linear characteristic to include saturation effects into the simulation. The non-linearity is usually numerically resolved by a Newton or fixed-point method (Hameyer and Belmans, 1999; Dlala *et al.*, 2008). Both methods can be applied to both the reference computation as well as the POD method. In this non-linear example the snapshots for the POD are equally distributed over the time interval. In contrast to that, the PGD is combined with the fixed-point method due to its separational approach. To be able to reduce the computational effort related to the evaluation of the non-linearity the DEIM is used in the POD and PGD. In the following, the reference and the POD solutions are obtained by the Newton method. The hybrid approach highly benefits from this possibility to evaluate reference solutions fast and the overall computational effort can be reduced.

In Figure 6, the simulation results are given. The torque is well approximated for all methods. Contrary to the previous problem, the convergence of the POD is faster than the convergence of the PGD. The POD projection operator constructed from three equivalently distributed snapshots is used in the hybrid process. The error of the hybrid approach is greater for the first two modes than those of the PGD and POD. The convergence for modes three to five shows similarities with the standard PGD, but with a lower absolute error. In the two-dimensional simulation, the hybrid enrichment process improved the PGD both in terms of computational effort as well as accuracy.

4.3 Evaluation of computational effort

The computational effort of the reference simulation, the PGD, POD and hybrid approach is compared in the following section. As a measure, the number of solvings of linear systems of equations is proposed to exclude the computational time of a specific processing unit. The comparison given in Figure 7 contains the evaluation for the linear transient problem using the $T - \Omega$ formulation and the non-linear simulation of the synchronous machine. The transient problem in combination with the AV formulation is excluded due to the occurring stability issues. The different methods conduct different types of computations, each

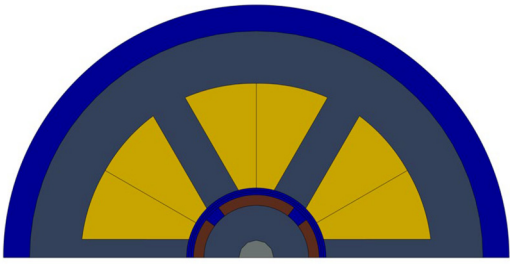

Source: Authors' own work

Figure 5.
Second case study – synchronous machine with surface mounted permanent magnets

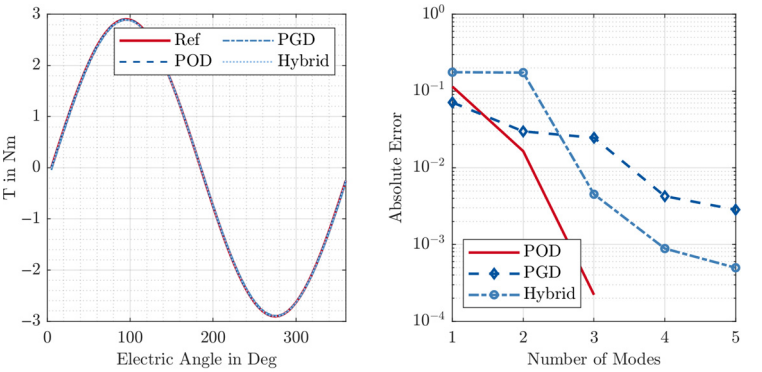

(a) **(b)**

Notes: (a) Torque versus electric angle; (b) absolute residual versus number of modes

Source: Authors' own work

Figure 6.
Non-linear locked rotor simulation results for the synchronous machine

holding a different amount of effort. To distinguish between these efforts, three bars (FEM, Red. FEM, Scal.) are assigned to each simulation type with the frequency of the respective efforts. In Figure 7(a), the "FEM" bar is obtained for the Ref and POD simulation from constructing and solving the system of equations (9) and (10). For the PGD and hybrid approach, it is achieved by setting up and solving the system of equations (20) and (21). The bar associated with "Scal." is connected to the effort of solving equations (22) and (23). In Figure 7, the standard FEM shows the largest computational effort. It is followed in terms of effort by a reduced computation, which is conducted by the POD in the reduced system or by applying the DEIM in the PGD. These computations are abbreviated by "Red. FEM" in the figures because the applied projection operators reduce the effort connected to building and solving the system of equations. The solving equations (22) and (23), denoted by "Scal.", to get the time functions in the PGD and hybrid approach holds the smallest computational burden. The effort of the linear problem given in Figure 7(a) and of the non-linear problem given in Figure 7(b) highlights the reduction of computational effort of the hybrid approach compared to the other methods. The factor of reduction compared to the reference computation of the linear problem is 8.57, respectively 2.1 for the non-linear problem. Additionally, the ratio of reduction compared to the standard PGD is 1.48 for the linear and 2.19 for the non-linear problem. Particularly for the non-linear problem, this reduction is interesting, because it decreases the number of solvings to be smaller than for the reference computation. For the transient problem one solving of scalar equations per used column of Ψ is conducted, but the non-linear problem needs to iteratively solve the scalar equations due to the ferromagnetic material characteristic.

5. Conclusion

A hybrid enrichment strategy is proposed to combine the advantages of the POD and PGD method for the computation of electromagnetic fields. The computation of different problem classes shows the reduction of computational effort of the PGD. Although the *a-priori* property of the PGD is lost, the computational reduction linear and non-linear problems can cope with this disadvantage of computing a small number of reference solutions. The achieved reduction factor in terms of effort compared to the standard FEM is 8.57 for the linear problem and 2.1 for the non-linear problem. Additionally to the

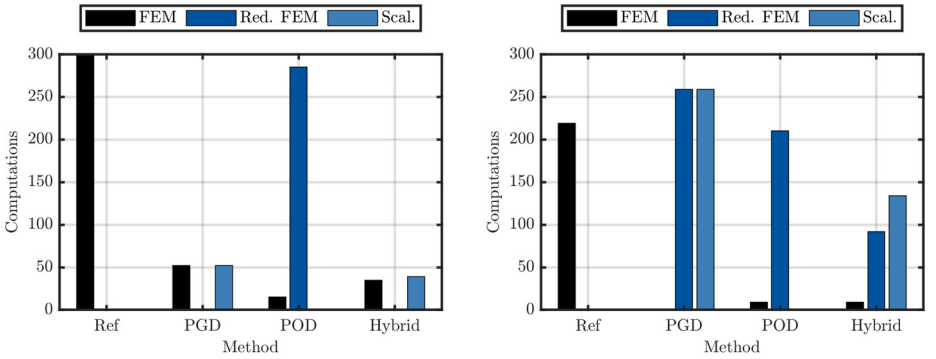

Figure 7. Comparison of number of finite element computations in terms of constructing and solving systems of equations; FEM: Full FE computation; Red. FEM: Solving of a system of equations in a reduced subspace; Scal.: Solving of equations to achieve the time functions

Notes: (a) Linear eddy current problem with T − Ω formulation; (b) non-linear problem with A-formulation

Source: Authors' own work

hybrid enrichment strategy, the PGD in combination with the AV formulation is derived. The results highlight that the separation approach of the PGD can be introduced in different formulations and the reduced model achieves accurate results. However, the hybrid approach for the PGD with the AV formulation shows unstable behavior and requires further research.

References

Boehmer, S., Lange, E. and Hameyer, K. (2013), "Non-conforming sliding interfaces for relative motion in 3D finite element analysis of electrical machines by magnetic scalar potential formulation without cuts", *IEEE Transactions on Magnetics*, Vol. 49 No. 5, pp. 1833-1836.

Chaturantabut, S. and Sorensen, D.C. (2010), "Nonlinear model reduction via discrete empirical interpolation", *SIAM Journal on Scientific Computing*, Vol. 32 No. 5, pp. 2737-2764.

Chinesta, F., Ammar, A., Leygue, A. and Keunings, R. (2011), "An overview of the proper generalized decomposition with applications in computational rheology", *Journal of Non-Newtonian Fluid Mechanics*, Vol. 166 No. 11, pp. 578-592.

Chinesta, F., Keunings, R. and Leygue, A. (2013), *The Proper Generalized Decomposition for Advanced Numerical Simulations: A Primer*, Springer Briefs, Berlin, Germany.

Clénet, S., Henneron, T. and Mac, H. (2015), "Error estimation of a proper orthogonal decomposition reduced model of a permanent magnet synchronous machine", *IET Science, Measurement and Technology*, Vol. 9 No. 2, pp. 172-177.

Dlala, E., Belahcen, A. and Arkkio, A. (2008), "A fast fixed-point method for solving magnetic field problems in media of hysteresis", *IEEE Transactions on Magnetics*, Vol. 44 No. 6, pp. 1214-1217.

Hameyer, K. and Belmans, R. (1999), "Numerical modelling and design of electrical machines and devices, advances in electrical and electronic engineering", Southampton: WIT Press, 1999, isbn: 1-85312-626-8.

Henneron, T. and Clénet, S. (2017), "Application of the proper generalized decomposition to solve MagnetoElectric problem", *IEEE Transactions on Magnetics*, Vol. 54 No. 3, pp. 1-4.

Henneron, T. and Clénet, S. (2016), "Application of the PGD and DEIM to solve a 3-D non-linear magnetostatic problem coupled with the circuit equations", *IEEE Transactions on Magnetics*, Vol. 52 No. 3, pp. 1-4.

Kasolis, F. and Clemens, M. (2020), "Entropy snapshot filtering for QR-based model reduction of transient nonlinear electro-quasi-static simulations", *IEEE Transactions on Magnetics*, Vol. 56 No. 2, pp. 1-4.

Krimm, A., Casper, T., Schöps, S., De Gersem, H. and Chamoin, L. (2019), "Proper generalized decomposition of parameterized electrothermal problems discretized by the finite integration technique", *IEEE Transactions on Magnetics*, Vol. 55 No. 6, pp. 1-4.

Kuczmann, M. and Iványi, A. (2008), *The Finite Element Method in Magnetics*, Akadémiai Kiadó, Budapest, isbn: 9630586495.

Montier, L., Pierquin, A., Henneron, T. and Clénet, S. (2017), "Structure preserving model reduction of low-frequency electromagnetic problem based on POD and DEIM", *IEEE Transactions on Magnetics*, Vol. 53 No. 6, pp. 1-4.

Mukherjee, V., Far, M.F., Martin, F. and Belahcen, A. (2017), "Constrained algorithm for the selection of uneven snapshots in model order reduction of a bearingless motor", *IEEE Transactions on Magnetics*, Vol. 53 No. 6, pp. 1-4.

Müller, F., Baumanns, P., Nell, M.M. and Hameyer, K. (2022), "Nonlinear parameteric simulation by proper generalized decomposition on the example of a synchronous machine", *COMPEL - The International Journal for Computation and Mathematics in Electrical and Electronic Engineering*, Vol. 41 No. 4, pp. 1171-1180.

Müller, F., Crampen, L., Henneron, T., Clénet, S. and Hameyer, K. (2020a), "Model order reduction techniques applied to magnetodynamic T-Ω-formulation", *COMPEL - The International Journal for Computation and Mathematics in Electrical and Electronic Engineering*, Vol. 39 No. 5, pp. 1057-1069.

Müller, F., Henneron, H., Clénet, S. and Hameyer, K. (2020b), "Error estimators for proper generalized decomposition in time-dependent electromagnetic field problems", *IEEE Transactions on Magnetics*, Vol. 56 No. 1, pp. 1-4.

Müller, F., Siokos, A., Kolb, J., Nell, M. and Hameyer, K. (2021), "Efficient estimation of electrical machine behavior by model order reduction", *IEEE Transactions on Magnetics*, Vol. 57 No. 6, pp. 1-4.

Nouy, A. (2010), "A priori model reduction through proper generalized decomposition for solving time-dependent partial differential equations", *Computer Methods in Applied Mechanics and Engineering*, Vol. 199 Nos 23/24, pp. 1603-1626.

Corresponding author
Fabian Müller can be contacted at: fabian.mueller@iem.rwth-aachen.de